Hydrol. Earth Syst. Sci. Discuss., 10, 3327–3381, 2013
www.hydrol-earth-syst-sci-discuss.net/10/3327/2013/
doi:10.5194/hessd-10-3327-2013

Hydrology and Earth System Sciences
Open Access
Discussions

Integrated assessment of global water scarcity over the 21st century – Part 1: Global water supply and demand under extreme radiative forcing

M. I. Hejazi[1], J. Edmonds[1], L. Clarke[1], P. Kyle[1], E. Davies[2], V. Chaturvedi[1], M. Wise[1], P. Patel[1], J. Eom[1], and K. Calvin[1]

[1]Joint Global Change Research Institute, Pacific Northwest National Laboratory, College Park, Maryland, USA
[2]Department of Civil and Environmental Engineering, University of Alberta, Alberta, Canada

Received: 31 January 2013 – Accepted: 15 February 2013 – Published: 13 March 2013

Correspondence to: M. I. Hejazi (mohamad.hejazi@pnnl.gov)

Published by Copernicus Publications on behalf of the European Geosciences Union.

Abstract

Water scarcity conditions over the 21st century both globally and regionally are assessed in the context of climate change, by estimating both water availability and water demand within the Global Change Assessment Model (GCAM), a leading community integrated assessment model of energy, agriculture, climate, and water. To quantify changes in future water availability, a new gridded water-balance global hydrologic model – namely, the Global Water Availability Model (GWAM) – is developed and evaluated. Global water demands for six major demand sectors (irrigation, livestock, domestic, electricity generation, primary energy production, and manufacturing) are modeled in GCAM at the regional scale (14 geopolitical regions, 151 sub-regions) and then spatially downscaled to $0.5^{\circ} \times 0.5^{\circ}$ resolution to match the scale of GWAM. Using a baseline scenario (i.e., no climate change mitigation policy) with radiative forcing reaching 8.8 W m^{-2} (equivalent to the SRES A1Fi emission scenario) and a global population of 14 billion by 2095, global annual water demand grows from about 9–10 % of total annual renewable freshwater in 2005 to about 32–37 % by 2095. This results in more than half of the world population living under extreme water scarcity by the end of the 21st century. Regionally, the demand for water exceeds the amount of water availability in two GCAM regions, the Middle East and India. Additionally, in years 2050 and 2095 36 % (28 %) and 44 % (39 %) of the global population, respectively is projected to live in grid cells (in basins) that will experience greater water demands than the amount of available water in a year (i.e., the water scarcity index (WSI) > 1.0). This study implies an increasingly prominent role for water in future human decisions, and highlights the importance of including water in integrated assessment of global change.

1 Introduction

The United Nations estimated in 1997 that approximately one third of the world's population was living in countries experiencing moderate to severe water stress (WMO,

HESSD
10, 3327–3381, 2013

1997). Water stress is generally assessed by comparing water availability to water demand at various spatial (e.g., grid, county, basin, country) and temporal (e.g., monthly, annual) scales (Arnell, 1999a, 2004; Vörösmarty et al., 2000; Oki et al., 2001; Alcamo and Henrichs, 2002; Alcamo et al., 2003; Islam et al., 2007; Viviroli et al., 2007; Wada et al., 2011). Several studies have also assessed water scarcity conditions in the future, with water demands modeled as a function of socioeconomic assumptions, and water availability derived using climate models (Arnell, 1999a, 2004; Vörösmarty et al., 2000; Alcamo et al., 2003b). In this study, we build on these previous assessments, computing water scarcity at the $0.5 \times 0.5^{\circ}$ grid scale in five-year time steps between 2005 and 2095, by incorporating the hydrologic system into an integrated assessment model of energy, agriculture, and climate (GCAM). However, rather than combining various models, this approach produces consistent scenarios, where all these systems are simulated simultaneously in an internally consistent framework, and this integration allows analysis of the interactions between water demands and availabilities and their implications on water scarcity conditions in the context of future energy use, agriculture and land use, and climate change.

Estimation of climate impacts on water scarcity hinges on our ability to quantify how climate change affects both water availability and water demand. The climate system regulates the amount of water being circulated in the terrestrial biosphere, and climate change is expected to accelerate water cycling, induce changes in seasonal patterns, and increase the frequency of extreme events (Oki and Kanae, 2006; Held and Soden, 2006; Huntington, 2006). Climate change and changes in land use and land cover are also expected to influence the amount, timing, and reliability of regional fresh water in different directions (Milly et al., 2005; Wang and Hejazi, 2011), and consequently, are likely to affect water supply resources (Rowan et al., 2011) by influencing the amount of runoff volume and groundwater recharge to replenish aquifers (Wada et al., 2010). Furthermore, any quantification of climate change impacts on water resources is incomplete without also incorporating human demands of water. In any river basin, future water demands will be influenced by changes in the number of humans, their income

HESSD
10, 3327–3381, 2013

levels, the production and consumption of goods, services and food, and the characteristics of the technologies used to supply goods, services, and food. Future water demands will be further affected by water use policies, technological change, and climate change mitigation policies designed to reduce emissions of greenhouse gases (GHGs) (Arnell et al., 2011).

For assessment of climate impacts on water, global hydrologic models are generally incorporated into general circulation models (GCMs), allowing spatially and temporally explicit quantification of changes in the water system over the upcoming century. The first such numerical parameterization of the hydrologic cycle within a GCM was done by Manabe (1969). However, the initially simplistic and coarse representation of the hydrologic cycle within a GCM resulted in poor hydrologic predictive skill (Kuhl and Miller, 1992; Miller and Russell, 1992). To alleviate this shortcoming, GCMs have utilized Land Surface Models (LSMs) with hydrologic capabilities to improve the representation of runoff. Oki et al. (2001,1999) argued that current LSMs can simulate monthly river runoff quite well, provided that the precipitation and other climate forcing input data for the LSMs are sufficiently accurate. However, many LSMs still remain too coarse to capture some underlying hydrologic processes. Thus, a group of sub-grid parameterization LSMs have emerged (e.g., VIC (Liang et al., 1994, 1996), SIMTOP (Niu et al., 2005), GBHM (Yang et al., 2001)). This group of models generally represents the sub-grid variability (in soil moisture storage capacity, topography, and/or vegetation) as a spatial probability distribution.

An alternative is the emergence of a family of global water-balance models (WBM/WBMplus (Vörösmarty et al., 1998, 1989), WATBAL (Kaczmarek, 1993; Yates, 1994, 1996), WaterGAP/WEHY (Alcamo et al., 2003a, 1997), macroPDM (Arnell, 1999b), IMPACT-WATER (Cai and Rosegrant, 2002), FAO's model (Bruinsma, 2003), LPJ/LPJmL (Gertena et al., 2004; Rost et al., 2008), GEPIC (Liu et al., 2007, 2009; Liu and Yang, 2010), WASMOD-M (Wide'n-Nilsson et al., 2007), WATERSIM (de Fraiture, 2007), H07/H08 (Hanasaki et al., 2006, 2007), and PCR-GLOBWB (Weiland et al., 2010) that improve the ability to simulate water availability on a global scale from GCM

HESSD
10, 3327–3381, 2013

climatic forcings. Those models have evolved from a vertical water balance at the grid scale (typically 0.5 × 0.5), to routing water spatially from one grid cell to another, incorporating crop growth models, and modeling global water management components (e.g., reservoir management, human water use). However, not all such models incorporate all of these details, and they vary with regard to temporal and spatial scale, runoff mechanism, crop growth modeling scheme, and the representation of human systems. In general, global water balance models compute the water fluxes and related processes, and employ soil water balances based on climate, land cover (cropland, pasture, natural vegetation) and soil information, on a grid cell basis, typically at 0.5° resolution. In several of the models that focus on agriculture, soil water content thresholds are set at which irrigation is triggered. Some models, such as GEPIC, extend further to include nutrient cycling, tillage and agronomics, simulating the effects of different agricultural management options (Hoff et al., 2010). Some models (GEPIC, LPJmL) internally calculate crop yields, while other models (GCWM, WBMplus) use (mostly country-based) crop production data from agricultural statistics. In this study, the latter approach is used.

Water balance models typically use monthly climate data from the Climate Research Unit (CRU, University of East Anglia) to simulate the hydrologic processes, but some models temporally downscale the climate input data to daily scale to better model crop growth and irrigation water demand. Land use is generally based on the Ramankutty et al. (2008) distribution and extent of cropland and permanent pasture. Areas equipped for irrigation are generally taken from Siebert et al. (2007) and crop types from Monfreda et al. (2008) or Portmann et al. (2008). Generally, land use is assumed constant over the duration of the simulation period. Furthermore, different approaches for calculating potential evapotranspiration (PET) are typically used in different models, e.g., Penman–Monteith (GCWM), Priestley–Taylor (GCWM, IMPACT, LPJmL, WaterGap), Hargreaves (GEPIC), Hamon (WBMplus), or bulk formulas (H08). Zomer et al. (2006) applied five methods of estimating potential evapotranspiration to South America and Africa and found that the Hargreaves method (Hargreaves et al.,

HESSD
10, 3327–3381, 2013

1985) compared favorably with the FAO Penman–Monteith, but required less parameterization, and with improved robustness to error in climatic inputs (Hargreaves and Allen, 2003). Thus, to determine agricultural water consumption in this study, we use the Hargreaves method.

Our primary goal in this study is to model water demand and supply in a unified and internally consistent integrated assessment framework that captures the inter-linkages and feedbacks with other natural and human systems, which can be exceptionally useful to assess the current and future picture of both global and regional water scarcity more accurately. This integrated modeling framework facilitates estimation of water resources demands and supplies globally and regionally by explicitly modeling the effects and feedbacks of both natural processes (climate model, crop model, and land use model) and human systems (anthropogenic forcing, land use change, energy demands and technologies, socioeconomics, and market-based economies). Thus, in this study, we incorporate a new gridded water-balance global hydrologic model (GWAM) as a new component to the GCAM water system, and combine with spatially downscaled representations of all the existing water demand sectors (Hejazi et al., 2013a, b; Chaturvedi et al., 2013; Davies et al., 2013) in GCAM to produce a dynamic, high-resolution view of global, annual water scarcity.

Next, we briefly describe GCAM, and present the methods of modeling global water availability and demands in GCAM, with special attention to the downscaling techniques.

2 GCAM

GCAM is a dynamic-recursive model combining representations of the global economy, the energy system, agriculture and land use, and climate. Exogenous inputs include (among other variables) present and future population, labor productivity, energy and agricultural technology characteristics, and resource availabilities. In its current implementation, GCAM has the following 14 geopolitical regions: the United States, Canada,

HESSD
10, 3327–3381, 2013

Western Europe, Japan, Australia and New Zealand, former Soviet Union, Eastern Europe, Latin America, Africa, Middle East, China (and Asian reforming economies), India, South Korea, and the rest of South and East Asia. The model is calibrated to historical energy, agricultural, land, and climate data through the 2005 time period, and runs in five-year time steps to 2095, establishing market-clearing prices for all energy, agriculture, and land markets such that supplies and demands of all modeled markets are in equilibrium. GCAM traditionally includes representations of the economic, energy, and land use systems, and uses the Model for the Assessment of Greenhouse-gas Induced Climate Change (MAGICC) (Raper et al., 1996; Wigley and Raper, 1992, 2002) as its reduced-form representation of the atmosphere, ocean and climate systems. The water system including both demand and supply are incorporated into GCAM as shown in Fig. 1.

3 Global water availability model (GWAM)

3.1 Model overview

In this study, a global hydrologic model, GWAM, is constructed, and evaluated. GWAM is designed to retain consistency with the approaches used in current state-of-the-art hydrological models, but with several modifications and simplifications in order to allow incorporation into GCAM. Components that are excluded in GWAM (as compared to most existing global hydrologic models) are river and reservoir routing, and a crop growth model that is simulated at the same temporal and spatial scale as the hydrology model. The former component is generally an important feature to achieve accurate monthly estimates of runoff, but it is less crucial when accounting for water on an annual basis and over very large first order basins that drain directly to non-fresh water bodies. This study incorporates a crop model similar to the FAO approach (FAO, 2001) since the agricultural water demand module is repeatedly calculated as GCAM solves

HESSD
10, 3327–3381, 2013

all the markets in a particular time period, thus reducing the computational burden tremendously.

GWAM reproduces historical streamflow observations and simulates the future availability of freshwater under both a changing climate and an evolving landscape with competing water users. The model is grid-based, with a spatial resolution of 0.5 × 0.5°, and a monthly time step. Water routing capabilities and reservoir operation rules are not included. The water supply model is first evaluated against observational data and other models, and then simulated into the future to provide estimates of total water supply up to the end of the 21st century.

The global water availability model provides estimates of renewable freshwater resources in the form of either surface flow or groundwater recharge. This indicates the maximum theoretical amount of water naturally available in a year for each of the basins. In reality, some of the runoff flows too quickly to saline water bodies or occurs in remote areas where there is no potential for people to use it. Thus, almost all recent studies have assessed water scarcity conditions using water scarcity indices such as that of Falkenmark (1989) and Raskin (1997). Wada et al. (2011) provide a detailed summary of previous studies that have also used the definition of Raskin, which compares total water demand to the total amount of renewable water available, and defines extreme water scarcity in any region as demand in excess of 40 % of total water availability. In regions where the total water demands exceed the total stable flow of renewable water, humans have tapped into other sources that are either quite expensive (desalination of brackish and saline water) or unsustainable (fossil groundwater abstractions) (Wada et al., 2010; Gleeson et al., 2012). In this paper, we only consider renewable water resources (i.e., annual flow of rivers and recharge of aquifers) in the water scarcity calculations.

3.2 Model structure

The global water availability model (GWAM) is a gridded monthly water balance model with a resolution of 0.5 × 0.5°. It requires gridded monthly precipitation, temperature,

HESSD
10, 3327–3381, 2013

and maximum soil water storage capacity (a function of land cover), and computes the amounts of evapotranspiration to the atmosphere, runoff, and soil moisture in the soil column. The model structure (Fig. 2) is consistent with existing global water balance models, and with the FAO's model formulation for modeling water resources in Africa (FAO, 2001). GWAM tracks the fraction of rainfall that feeds into the soil column (green water) and runoff (blue water) at a monthly scale. The model accounts for the monthly green water storage and estimates the fraction of green and blue water that is evaporated back to the atmosphere through evapotranspiration from vegetation and cultivated lands and evaporation from bare soil or water bodies. The maximum soil moisture storage capacity (S_m) with a resolution of $0.5 \times 0.5^\circ$ is obtained from the soil map of the world and soil properties (FAO, 1998, 2003). Information with regard to the "maximum soil moisture storage capacity" in $\mathrm{mm\,m^{-1}}$ is derived from the "Derived Soil Properties" of the "Digital Soil Map of the World" which contains raster information on soil moisture in different classes (FAO, 1998, 2003). Maximum available soil moisture is estimated from estimates of root depth, field capacity, and wilting point values (typically ranges between 15–350 $\mathrm{mm\,m^{-1}}$). The root depth estimate is itself a function of land cover and water stress conditions. In this study, a static S_m map over time is assumed.

As with any water balance model, the conservation of mass is observed following Eq. (1). That is, the amount of storage in the soil column (S_t) is the sum of initially available water in storage (S_{t-1}) plus the amount of precipitation that falls during the month, minus the amount of water that evaporates back to the atmosphere through evaporation from water bodies or the soil, or through transpiration from vegetation (AET_t) and the amount of runoff (Q_t) during the month t.

$$S_t = S_{t-1} + P_t - \mathrm{AET}_t - Q_t \quad (1)$$

More specifically, for any given month and grid cell, the amount of water available ($S_{t-1} + P_t - \mathrm{PET}_t$) in any month t is a function of the amount of new precipitation P_t, the amount of water available in storage S_{t-1}, and potential evapotranspiration PET_t. However, the amount of water actually returned to the atmosphere is generally less

HESSD
10, 3327–3381, 2013

than the amount potentially available due to water stresses; i.e., the amount of water available in the soil column is less than the estimated PET_t value in a particular grid (an effect particularly apparent in desert and semi-arid regions). Thus, the amount of actual evapotranspiration (AET_t) is modeled in theory as a function (Eq. 2) of the potential evapotranspiration as derived from climatic forcings, adjusted based on the water availability in a particular grid for a particular month. A nonlinear equation (Eq. 3) is used to determine actual evapotranspiration as a function of PET and the relative soil moisture state in a grid cell, according to Kaczmarek (1993).

$$AET_t = \beta \cdot PET_t \tag{2}$$

$$\beta = \left(\frac{5 \cdot \left(\frac{S_{t-1}}{S_m}\right) - 2 \cdot \left(\frac{S_{t-1}}{S_m}\right)^2}{3} \right) \tag{3}$$

In practice, we estimate AET_t following Eq. (4).

$$AET_t = \begin{cases} PET_t & S_{t-1} + P_t - PET_t \geq S_m \\ \beta \cdot PET_t & 0 \leq S_{t-1} + P_t - \beta \cdot PET_t < S_m \\ S_{t-1} + P_t & S_{t-1} + P_t - \beta \cdot PET_t < 0 \\ 0.1 \cdot PET_t & \beta \leq 0.1 \end{cases} \tag{4}$$

Once AET_t is estimated, the current amount of storage can be computed following Eq. (5).

$$S_t = \begin{cases} S_m & S_{t-1} + P_t - PET_t \geq S_m \\ \gamma \cdot S_{t-1} + P_t - AET_t & \text{otherwise} \\ 0 & \gamma \cdot S_{t-1} + P_t - AET_t < 0 \end{cases} \tag{5}$$

HESSD
10, 3327–3381, 2013

Where, γ is a unitless drying function of the soil column following the WBM formulation (Vörösmarty et al., 1998).

$$\gamma = \left(\frac{1 - e^{-\alpha \frac{S_{t-1}}{S_m}}}{1 - e^{-\alpha}} \right) \quad (6)$$

Where α is an empirical constant (set to 1.0) and γ is the soil and vegetation-dependent available water capacity (Vörösmarty et al., 1998).

Finally, having estimated AET_t and S_t and given the values of S_{t-1} (estimated in previous time step) and P_t (an input variable), Eq. (1) can be rearranged to compute Q_t

$$Q_t = S_{t-1} + P_t - \mathrm{AET}_t - S_t \quad (7)$$

Then the storage value of each grid cell is updated, the time index is incremented by one month, and the calculation procedure is repeated until the end of the simulation period. Figure 3 shows a detailed flowchart schematic of the model calculation algorithm. Details of calculating monthly PET (Hargreaves Method) are summarized in Appendix A.

To simulate GWAM both historically (1901–2002) and in the future (2001–2100), gridded monthly climatic input variables are taken from the Climate Research Unit (CRU TS 2.0, Mitchell et al., 2004), and from the Tyndall Centre for Climate Change Research (TYN SC 2.1, Mitchell and Jones, 2005), respectively, both at the University of East Anglia.

3.3 Model evaluation

Prior to simulating GWAM into the future, the model ability to reproduce historical values is evaluated against observations, statistical assessments, and other global hydrologic models. Globally, the mean annual runoff of 38 587 $\mathrm{km^3\,yr^{-1}}$ is similar to previous

HESSD
10, 3327–3381, 2013

data-based and model-based estimates, as shown in Fig. 4. Figure 5 shows a comparison between our average annual runoff at the continental scale with other data-based and model estimates. The simulated global and continental mean annual runoff ranges correspond to the ranges of previous studies. The range bar around our estimates denotes the maximum and minimum annual runoff during the historical simulation period (1901–2002) for the global (Fig. 4) and continental (Fig. 5) scales. Note that, globally, data-based estimates are higher on average than model-based estimates. The observed difference at the global and continental scales can arise due to variations in the simulation period and modeling approach. Discrepancies may also arise due to inconsistency of spatial coverage. For example, data-based estimates generally cover small islands while model based estimates ignore those regions due to lack of appropriate spatial resolution, as is the case with GWAM's scale of $0.5 \times 0.5^{\circ}$, which is generally too coarse to model small islands. Furthermore, some studies, including ours, do not include Greenland or Antarctica in the global and continental estimates. One additional source of variation at the continental scale may be due to how different studies split Russia between Asia and Europe. Table 1 summarizes the global and continental estimates from the literature.

Next, we compare our results in Fig. 6 with those of several other global hydrologic models (e.g., WBM (Fekete et al., 2000), WBMc (Fekete et al., 2000), and WGHM, Döll and Fiedler, 2008), and withthe FAO AQUASTAT estimates of renewable water resources by country, aggregated by GCAM regions in the year 2005 (AQUASTAT, 2012). Specific estimates for the country and GCAM regional scales are summarized in Tables S1 and 1, respectively. Table 2 presents estimates of the models' departure from FAO's estimates at the country scale (only countries for which all four models have values are used) and the GCAM regional scale; model departure is measured in terms of root mean squared error (RMSE). Overall, all models exhibit a similar range of goodness-of-fit (Table 3). Variations among the models may be due to variations in the representation of rainfall-runoff generation and how PET is computed.

HESSD
10, 3327–3381, 2013

Finally, we compare our simulation results of historical average annual runoff for 29 major basins of the world against observed values from the Global Runoff Data Centre (GRDC, 1999) – see Tables S2 and S3 for a complete summary of our results in comparison with several other data-based and model-based estimates. Figure 7 shows a scatter plot of the basin scale results in comparison to several other model results. Overall, models tend to overestimate small annual runoff values for the selected basins. Variations again could arise due to several factors. Delineated drainage areas are somewhat inconsistent and area differences are relatively large for some basins (this is not a concern for the comparison with WBM and WBMc because they use the same drainage areas). Second, the time of record and simulation periods differ across sources. Third, this study assumes natural conditions while observed runoff data capture other factors (e.g., human activities). Thus, GWAM generally overestimates water availability (i.e., annual runoff) as compared with observed data in basins where water consumption is extensive (especially agricultural water consumption) relative to water supply.

3.4 GWAM future simulations

GWAM is simulated over the entire 21st century usingthe SRES (2000) A1Fi emission scenario and data from four GCMs (HadCM3, CSIRO2, CGCM2, PCM) (TYN SC 2.1, Mitchell and Jones, 2005). In this study, we use the GCM ensemble mean annual runoff to establish the amount of maximum theoretically available renewable water at any grid cell in any month. GCM data are also used to quantify the effect of climate model uncertainty on the amount of water availability, and subsequently, water scarcity conditions. Figure 8 shows the grid-based mean annual runoff in years 2000, 2050, and 2095; annual values are averaged over 1996–2002, 2046–2055, and 2091–2100, respectively. The latter two periods are ensemble mean annual runoff values based on using four GCMs to simulate GWAM in the future. Next we describe the global water demand model.

HESSD
10, 3327–3381, 2013

4 GCAM – global water demand model (GWDM)

4.1 Model overview

Recently, Hejazi et al. (2013b) explicitly incorporated sectoral water demand modules within the framework of GCAM to estimate the amount of freshwater demanded on an annual basis. The water demand modules account for water use for irrigation, livestock, domestic purposes, electricity generation, primary energy production, and manufacturing. The modules have been constructed, calibrated, and evaluated (Hejazi et al., 2013b). Future agricultural water demands are driven by crop production from GCAM and the share of crop production that takes place on irrigated lands, by up to 18 agro-ecological zones (AEZ) within 14 geopolitical regions (151 sub-regions), and by crop type (12 types). Future manufacturing and domestic water demands are driven by scenario-specific socioeconomic assumptions (e.g., population, GDP), among other factors. Water demands for primary energy are scaled with the amount of each fuel produced, and water demands for secondary energy (electricity, refined liquid products) depend on the specific production technologies used. In the electric sector in particular, water use depends not only on the generation technology mix, but also on the types of cooling systems used, for which we make explicit assumptions. Thus, in this study, water demands are modeled for the agricultural, industrial, and municipal sectors, using technology-based representations where possible. Figure 1 shows how each of the six water demand sectors are linked to the existing systems in GCAM.

In this study, socioeconomic characteristics and emissions prices are adjusted so that the GCAM output for radiative forcing matches that associated with the SRES A1Fi emission scenario. This adopted scenario reflects a world with no emissions mitigation (similar to the POP14/MDG-scenario in Hejazi et al., 2013b); as such, it can be considered a baseline scenario, with no climate change mitigation policy. A companion paper (Hejazi et al., 2013c) will investigate how different climate change mitigation policies could impact future water scarcity conditions. The adopted scenario in this paper is characterized by growth from 2005 to 2095 in world population from 6.5 billion

HESSD
10, 3327–3381, 2013

to 13.7 billion, and per capita GDP from 4607 to 28 136 (1990 US$). In spite of assumed technological improvements, global energy consumption increases from 458 EJ to 2236 EJ. Figure 9 shows the estimated total water demand by sector plotted along with the total water available globally. Globally, total annual demand grows from about 9–10 % of total annual available to about 32–37 % by 2095. This dramatic growth in water demand is likely to cause widespread water scarcity in many regions by the end of the century. Irrigation water demands remain the dominant use of water globally over the entire century, followed by the industrial, and then domestic sectors. Next, we downscale the GCAM water demand results to grid scale using available spatial assessments of population, livestock, and irrigation.

4.2 Spatial downscaling to grid scale

The overarching goal of this study is to link the global water supply and demand models described above to GCAM's existing energy, agricultural, and socioeconomic systems. However, the spatial resolution of these existing systems in GCAM is not adequate for detailed analysis of the water system; to link these systems, spatial downscaling of GCAM output is necessary. In this paper, we separately downscale irrigation water demands, livestock water demands, and all remaining water demands (e.g., municipal, electricity generation, primary energy, and manufacturing water demands). For the latter, we use population to downscale water demand estimates from the 14 GCAM regions to the grid scale ($0.5 \times 0.5^{\circ}$). Using the WWDR-II population data (Elvidge et al., 1997a, b; ESRI, 1993; Tobler et al., 1995) and following the work of Wada et al. (2011), the population gridded map is converted to population density maps. Assuming that population density maps remain static over time within each GCAM region, and using the population projections for each GCAM region, a global map of gridded population is generated for every GCAM modeling period (e.g., 2005, 2010,. . . , 2095). Note that in this study, water scarcity conditions are assessed at the grid and basin scales. Note also that the downscaling technique does not allow for population diffusion into currently unpopulated areas, an assumption which may tend to overestimate water

HESSD
10, 3327–3381, 2013

scarcity at the grid scale. Figure 10 shows the total gridded non-agricultural water demand in years 2005, 2050, and 2095. The increases in India and Eastern China are most pronounced.

Similarly, irrigation water demand is downscaled to a $0.5 \times 0.5^{\circ}$ grid using existing global coverage of gridded information of crop areas equipped with irrigation in the year 2000 and the corresponding fraction of coverage of each grid area (both from Siebert et al., 2007) and by crop type (from Portmann et al., 2008). Recall that GCAM computes irrigation water demand at the AEZ scale (151 regions globally). Also, the amounts of new irrigated lands in each crop, AEZ, and GCAM region and the corresponding total irrigation volume are known from GCAM for each 5-yr interval period between 2005 and 2095. First, starting with the base year estimates, the fraction of irrigated land in each grid is scaled up linearly to account for the additional irrigated lands. When the fraction of irrigated land in a grid cell reaches 100 %, the remaining additional irrigated lands are distributed uniformly across the remaining grid cells that are classified as equipped with irrigation. When all grid cells equipped with irrigation are fully irrigated or when irrigation emerges in sub-regional AEZs where no grid cells equipped with irrigation currently exist, irrigated lands are distributed uniformly across all arable lands. Using the density map of the share of irrigated lands and the required irrigation volume, and projecting them into the future, one can estimate the amount of irrigation downscaled to the grid scale. As shown in Fig. 11, regions such as Northern India, Northeastern China, and Southeastern Asia face dramatic increases in irrigation water demand in this scenario.

To downscale livestock water demand, we follow the work of Alcamo et al. (2003a), Flörke and Alcamo (2004), and Wada et al. (2011) in utilizing the gridded global maps of estimated livestock density for six major livestock types (cattle, buffalo, sheep, goats, pigs, and poultry) in year 2000 (Wint and Robinson, 2007). Projecting into the future, the amount of water used is scaled up assuming the density maps to remain static within each GCAM region. Figure 12 shows the global livestock demand spatially in years 2005, 2050, and 2095. With higher population growth and greater demand for

HESSD
10, 3327–3381, 2013

food (dairy and meat), places such India, China, Central Africa, and Brazil experience the largest increase in livestock water demand by the end of the 21st century. Note, livestock water demand is relatively minor in comparison with the total non-agricultural (Fig. 10) and irrigation (Fig. 11) water demands. Figures 13 and 14 show the global agricultural water demand (irrigation and livestock) and total water demand (agricultural and non-agricultural) estimates in years 2005, 2050, and 2095. The greatest increase in water demand is concentrated around Northern India and Eastern China.

5 Water scarcity

Next, we quantify the effect of climate change on water scarcity both globally and in each of the GCAM regions. To estimate water scarcity, we adopt the Raskin's definition of water scarcity (Raskin et al., 1997) as the ratio of total water withdrawal (TWW) to total water availability (TWA); i.e., WSI = $\frac{\text{TWW}}{\text{TWA}}$. This definition of water scarcity is sometimes referred to in the literature as the water resources vulnerability index (WRVI), the withdrawal-to-availability (WTA) ratio, and the criticality ratio (Brown and Matlock, 2011). Following previously suggested thresholds for water scarcity conditions (Falkenmark, 1999; Falkenmark et al., 2007), WSI is divided up into four categories: no scarcity (WSI < 0.1) low scarcity ($0.1 \leq$ WSI < 0.2), moderate scarcity ($0.2 \leq$ WSI < 0.4) and severe scarcity (WSI ≥ 0.4). To be consistent with the temporal and spatial scale of GWAM, water demand (withdrawals) results are downscaled from the GCAM output scale (GCAM 14 regions, or 151 AEZ scale) to establish water scarcity for each grid on a mean annual basis.

Given the grid-level estimates of both total annual water demand and availability, one can estimate the level of scarcity at the grid and basin scales with global coverage for each GCAM simulation period. Figure 15 shows the values of the water scarcity index at the grid (Fig. 15a) and basin (Fig. 15b) scales in years 2005, 2050, and 2095. Note that a value close to one indicates extreme water stress conditions while a value close to zero indicates abundant water resources as compared to demands. Generally,

HESSD
10, 3327–3381, 2013

the gridded global water scarcity map (Fig. 15a) is spatially consistent with the corresponding total demand map (Fig. 14). Similar pattern emerge from the basin scale water scarcity results (Fig. 15b). Since it is not clearly apparent from Fig. 8 how water availability has changed spatially over time, Fig. 16 shows the change in total water demands (Fig. 16a), total water availability (Fig. 16b), and water scarcity index at the grid (Fig. 16c) and basin scales (Fig. 16d) between 2095 and 2005. Although water demands increase most dramatically in India and eastern China (Fig. 16a), they are somewhat alleviated with increasing water availability according to the ensemble mean total annual water availability in those regions (Fig. 16b). Change in water availability also exhibits an overall increase in higher latitudes and a reduction in Eastern US, Brazil, and Southern Europe. Thus, more regions experience similar or elevated water scarcity conditions (Fig. 16c, d). Regionally, India, China, and the Middle East observe the largest increase in scarcity. In contrast, regions such as Canada, USA, Eastern Europe, and the Former Soviet Union exhibit little change from current conditions. This could be due to a compounded effect of more runoff in the higher latitudes, saturated growth in water demands, along with somewhat milder population and economic growth projections. The water demand results are expected to be sensitive to the underlying socioeconomic assumptions (among other assumptions, such as technological change) associated with the adopted emission scenario (e.g., A1fi). The impact of using several emission scenarios on water scarcity will be investigated in the companion paper (Hejazi et al., 2013c).

Aggregating water scarcity globally, Fig. 17a, b show the likely shifts to the cumulative probability density function of the fraction of global population living under different levels of scarcity (WSI) at the grid and basin scales, respectively. The thin lines reflect the uncertainty corresponding to any single climate model of the four GCMs instead of the ensemble mean of total annual water availability. Global populations living under severe water stress conditions at the grid scale (basin scale) increase from 40 % (29 %) in year 2005 to 53 % (56 %) and 62 % (64 %) in years 2050, and 2095, respectively; i.e., more than half of the world population will live under severe scarcity

HESSD
10, 3327–3381, 2013

conditions in year 2050. Table 4 summarizes the proportion of global population living under each water scarcity category. When compared to previous estimates from the literature (Wada et al., 2011) (and references therein) for current population experiencing scarcity conditions (1995–2000), our estimates in year 2005 fall within the documented range. The range of results signifies the wide level of uncertainty in such estimates. Uncertainty could arise from the method of estimating total water availability, to water demand projections, to spatial and temporal scale of water scarcity calculations, and to how demands are downscaled to the appropriate scale.

Figure 18 shows the distributions of global populations facing each of the four levels of water scarcity. Note that WSI values are computed at the grid and basin scales and then aggregated to the global scales. Regardless of the adopted scale of calculating WSI and the associated populations, both panels in Fig. 18 show an increasing proportion of global population living severe water stress under both the ensemble mean and all individual GCMs. Figure 19a, b show the evolution of the fraction of global population living severe water stress (WSI ≥ 0.4) when computing WSI at the grid and basin scales, respectively. The dashed lines represent the result associated with an individual GCM instead of the ensemble mean. The grid scale results (in comparison to basin scale results) tend to overestimate the water scarcity condition at the beginning century, but the difference between the grid and basin scale results diminishes towards the end of the century; i.e., the fraction of global population living severe water stress range between 60 % and 70 % by the end of the 21st century (Fig. 19).

6 Discussion and conclusions

For assessing global water scarcity under current and future scenarios, there are several unique advantages to the approach adopted in this study. Most previous modeling efforts have focused on specific components of the human–earth system and assumed the behavior of remaining components by applying projected trends, output of other models, or reanalysis data. In contrast, in this study, we model water demand and

HESSD
10, 3327–3381, 2013

availability within an internally-consistent integrated assessment modeling framework with structural representations for the demands of water in most of the major water demand sectors. Thus, both water demand and supply are driven from the same set of assumptions about population and income growth, technological change, and emission scenario. This is important because human society and the natural environment are inter-connected: changes to the climate and natural systems will require society to adapt, and its adaptation efforts will affect the global environment in return. This interplay between natural and socio-economic systems determines the entire system's evolution and makes the representation of the corresponding feedbacks critical to the development of appropriate adaptation and mitigation strategies (Davies and Simonovic, 2011).

Additionally, reconciling water demand and supply in an internally consistent integrated assessment framework represents an important advance in the integrated assessment modeling field, as water is generally not explicitly modeled. With water balancing in GCAM, one can tackle the question of the adequacy of water availability under different climate change mitigation policies. This is investigated in the companion paper (Hejazi et al., 2013c). Hejazi et al. (2013b) investigated the level of water demands in each GCAM region by the end of the 21st century under a set of six representative socioeconomic scenarios while assuming constant water availability to current condition. In this paper, we extend that work by incorporating a global water availability model in GCAM to capture the effect of climate change on the amount of available water in conjunction of demands. The impact of climate change on water demands are not accounted for, and the water demand scenario in this study is a slightly modified version of the POP14/MDG- scenario in Hejazi et al. (2013b) to match closely the emission trajectory used in simulating the global hydrologic model (e.g., SRES A1Fi). Hejazi et al. (2013b) found that the Middle East's and Indi's water demands have already or will exceed their annual renewable water availability during the 21st century. The incorporation of the global hydrologic model (i.e., the effect of climate change on hydrology) did not change the previous outcome. Thus, although spatially the amount

HESSD
10, 3327–3381, 2013

of water available changes over time (see Fig. 16b), growing water demand pressures generally impose a stronger influence on water scarcity conditions especially in regions such as India and the Middle East. These high water scarcity values indicate that the scenario is likely infeasible from a water perspective, since such high water stress would typically lead to the adoption of water conservation technologies, with implications for other human choices (e.g., food, energy). Again this signifies the importance of incorporating water demand and supply modules in integrated assessment models. Thus, future research should be directed at incorporating water shortage feedbacks in GCAM to understand better how such stresses will propagate across the various human and natural systems in GCAM.

When comparing water demand and supply at large regional scales, water scarcity is likely to be averaged out, as GCAM regions that contain much more water available than demanded annually may still encompass sub-regions or grids that experience extreme stress conditions. To better characterize scarcity, in this study we downscale the water demands from the GCAM regions and AEZs to the grid scale. Many grid cells exhibit higher water demands than the amount of runoff available. As shown in Fig. 17, the percentage of global population experiencing WSI > 1.0 (i.e., TWD > TWA) increases from 8–23 % in 2005 to 28–36 % and 39–44 % in years 2050 and 2095, respectively; the higher range estimates are associated with grid-based estimates of WSI (Fig. 17a). Note however that because large population densities tend to occur at the main stem of large rivers that drain large regions, and because river routing is not implemented in GWAM, results are likely to overestimate the percentage of populations facing water scarcity conditions. Thus, water scarcity calculations are also performed at the basin scale to complement the grid scale results. Also, the results in this paper reflect an extreme population scenario, and water scarcity is likely to be alleviated when testing less populated scenarios. The effects of different socioeconomic and emissions scenarios on global water scarcity assessments are not fully understood, but are likely to influence water scarcity conditions. Furthermore, although Table 4 indicates that the scarcity estimates in 2005 are still within the range of uncertainty in current estimates,

HESSD
10, 3327–3381, 2013

the projected estimates in scarcity along with the cited literature values exhibit a wide range of uncertainty. Thus, quantifying the various sources of uncertainty is an important step to improve the reliability of water scarcity estimates in the future.

Uncertainty in water scarcity estimates could arise from several factors, such as: the amount of water available (i.e., model uncertainty of global hydrologic models and GCM predictions), the adopted socioeconomic and technology assumptions, projections of global water demands, downscaling techniques of water demands to match the scale of the water availability modeling exercise (watershed or grid), and the adopted spatial and temporal resolutions at which water scarcity is computed. Studies that perform inter-model comparisons among global hydrologic models can help identify the major sources of uncertainty in water availability estimates. Gleick (2003) and Hejazi et al. (2013b) concluded that there is a wide range of variations in global water demand projections. Wada et al. found that shorter temporal scale leads to higher estimates of water scarcity globally, but their observed variation is still smaller than the level of variations observed in the literature. Finally, downscaling techniques are generally simplistic and more advanced models that capture migration and population dynamics, and more accurate downscaling of industrial (e.g., energy, electricity, and manufacturing) water demands are warranted.

Appendix A

Monthly pet calculations (Hargreaves method)

The following equations describe the calculations of monthly potential evapotranspiration (PET_m) using the Hargreaves method. First, PET is computed at the daily scale using Eq. (A1).

$$PET_d = 0.0023 \cdot Ra \cdot (T_a + 17.8) \cdot T_r^{0.5} \quad \text{(A1)}$$

HESSD
10, 3327–3381, 2013

where PET_d is the potential evapotranspiration in mm day^{-1}. To convert to monthly (PET_m), PET_d is multiplied by the number of days (n) in each month ($PET_m = n \cdot PET_d$). T_a is the average daily temperature in Celsius. T_r is the range between maximum and minimum daily temperatures in Celsius. Ra is the extraterrestrial solar radiation in mm day^{-1}.

$$Ra = \frac{(24)\cdot(60)}{\pi}\lambda \cdot G_{sc} \cdot d_r \cdot \left[w_s \cdot \sin(\varphi)\cdot\sin(\delta) + \cos(\varphi)\cdot\cos(\delta)\cdot\sin(w_s)\right] \quad \text{(A2)}$$

λ is the corresponding equivalent evaporation to convert Ra from MJ m^{-2} day^{-1} to mm day^{-1} ($\lambda = 0.408$), G_{sc} is the solar constant ($G_{sc} = 0.0820$ MJ m^{-2} min^{-1}), d_r is the inverse relative distance Earth–Sun, w_s is the sunset hour angle (in radians), φ is the latitude (in radians), and δ is the solar declination (in radians). The inverse relative distance Earth–Sun (d_r) is computed using Eq. (A3), where J is the number of the day in the year between 1 (1 January) and 365 (31 December).

$$d_r = 1 + 0.33\cdot\cos\left(\frac{2\pi}{365}\cdot J\right) \quad \text{(A3)}$$

Solar declination (δ) is the line of latitude over which the sun is directly overhead on any given day. Solar declination changes day to day due the Earth's revolution around the Sun and is computed using Eq. (A4).

$$\delta = 0.409\cdot\sin\left(\frac{2\pi}{365}\cdot J - 1.39\right) \quad \text{(A4)}$$

The sunset hour angle (w_s) (in radians) is computed using Eq. (A5).

$$w_s = \arccos(-\tan(\varphi)\cdot\tan(\delta)) \quad \text{(A5)}$$

Equation (A2) can be simplified by replacing all constants with a single coefficient.

$$Ra = 15.392\cdot d_r \cdot \left[w_s \cdot \sin(\varphi)\cdot\sin(\delta) + \cos(\varphi)\cdot\cos(\delta)\cdot\sin(w_s)\right] \quad \text{(A6)}$$

HESSD
10, 3327–3381, 2013

Supplementary material related to this article is available online at: http://www.hydrol-earth-syst-sci-discuss.net/10/3327/2013/hessd-10-3327-2013-supplement.pdf.

Acknowledgements. The authors are grateful for research support provided by the Integrated Assessment Research Program in the Office of Science of the US Department of Energy (DOE SC-IARP). This research used Evergreen computing resources at the Pacific Northwest National Laboratory's Joint Global Change Research Institute at the University of Maryland in College Park, which is supported by DOE SC-IARP. Pacific Northwest National Laboratory is operated by Battelle for the US Department of Energy under contract DE-AC05-76RL01830. The views and opinions expressed in this paper are those of the authors alone.

References

Alcamo, J. and Henrichs, T.: Critical regions: a model-based estimation of world water resources sensitive to global changes, Aquat. Sci., 64, 352–362, doi:10.1007/pl00012591, 2002.

Alcamo, J., Döll, P., Kaspar, F., and Siebert, S.: Global Change and Global Scenarios of Water Use and Availability: an Application of WaterGAP1.0, University of Kassel, Germany, 1997.

Alcamo, J., Doli, P., Henrichs, T., Kaspar, F., Lehner, B., Rosch, T., and Siebert, S.: Development and testing of the WaterGAP 2 global model of water use and availability, Hydrolog. Sci. J., 48, 317–337, doi:10.1623/hysj.48.3.317.45290, 2003a.

Alcamo, J., Döll, P., Henrichs, T., Kaspar, F., Lehner, B., Rösch, T., and Siebert, S.: Global estimates of water withdrawals and availability under current and future "business-as-usual" conditions, Hydrolog. Sci. J., 48, 339–348, doi:10.1623/hysj.48.3.339.45278, 2003b.

AQUASTAT Database: FAO's global information system on water and agriculture: available at: http://www.fao.org/nr/water/aquastat/main/index.stm, (last access: March 2013), 2012.

Arnell, N.: Climate change and global water resources, Global Environ. Chang., 9, Suppl. 1, S31–S49, doi:10.1016/s0959-3780(99)00017-5, 1999a.

Arnell, N.: A simple water balance model for the simulation of streamflow over a large geographic domain, J. Hydrol., 217, 314–335, doi:10.1016/s0022-1694(99)00023-2, 1999b.

HESSD
10, 3327–3381, 2013

Arnell, N.: Climate change and global water resources: SRES emissions and socio-economic scenarios, Global Environ. Chang., 14, 31–52, doi:10.1016/j.gloenvcha.2003.10.006, 2004.
Arnell, N., van Vuuren, D., and Isaac, M.: The implications of climate policy for the impacts of climate change on global water resources, Global Environ. Chang., 21, 592–603, doi:10.1016/j.gloenvcha.2011.01.015, 2011.
Bruinsma, J. E.: World Agriculture: Towards 2015/2030 – an FAO Perspective, FAO, Rome, London, 2003.
Cai, X. and Rosegrant, M. W.: Global water demand and supply projections, Part 1: A modeling approach, Water Int., 27, 159–169, 2002.
Chaturvedi, V., Hejazi, M., Edmonds, J., Clarke, L., Kyle, P., Davies, E., Wise, M., and Calvin, K.: Climate policy implications for agricultural water demand, Climate Policy, in review, 2013.
Davies, E. and Simonovic, S.: Global water resources modeling with an integrated model of the social–economic–environmental system, Adv. Water Resour., 34, 684–700, doi:10.1016/j.advwatres.2011.02.010, 2011.
Davies, E., Kyle, P., and Edmonds, J.: An integrated assessment of global and regional water demands for electricity generation to 2095, Adv. Water Resour., 52, 296–313, 2013.
de Fraiture, C.: Integrated water and food analysis at the global and basin level. An application of WATERSIM, Water Resour. Manag., 21, 185–198, doi:10.1007/s11269-006-9048-9, 2007.
Döll, P. and Fiedler, K.: Global-scale modeling of groundwater recharge, Hydrol. Earth Syst. Sci., 12, 863–885, doi:10.5194/hess-12-863-2008, 2008.
Elvidge, C. D., Baugh, K. E., Kihn, E. A., Kroehl, H. W., and Davis, E. R.: Mapping city lights with nighttime data from the DMSP operational linescan system, Photogramm. Eng. Rem. S., 63, 727–734, 1997a.
Elvidge, C. D., Baugh, K. E., Kihn, E. A., Kroehl, H. W., Davis, E. R., and Davis, C. W.: Relation between satellite observed visible-near infrared emissions, population, economic activity and electric power consumption, Int. J. Remote Sens., 18, 1373–1379, doi:10.1080/014311697218485, 1997b.
ESRI: The Digital Chart of the World, Environmental Systems Research Institute Redlands, California, 1993.
Falkenmark, M.: The massive water scarcity now threatening Africa: why isn't it being addressed?, Ambio, 18, 112–118, 1989.

HESSD
10, 3327–3381, 2013

Falkenmark, M.: Forward to the future: a conceptual framework for water dependence, Ambio, 28, 356–361, 1999.
Falkenmark, M., Berntell, A., Jägerskog, A., Lundqvist, J., Matz, M., and Tropp, H.: On the Verge of a New Water Scarcity: a Call for Good Governance and Human Ingenuity, Stockholm Int. Water Inst., Stockholm, 2007.
FAO: Digital Soil of the World and Derived Soil Properties, FAO, Rome, 1998.
FAO: Water Resources and Irrigation in Africa, initially published in "Atlas of Water Resources and Irrigation in Africa (CD-ROM)", FAO, Rome, 2001.
FAO: Digital Soil Map of the World and Derived Soil Properties, Version 3.5 Edn., FAO, Rome, Italy, 2003.
Fekete, B. M., Vörösmarty, C. J., and Grabs, W.: Global Composite Runoff Fields Based on Observed River Discharge and Simulated Water Balances, Global Runoff Data Centre, Koblenz, Germany, 2000.
Flörke, M. and Alcamo, J.: European Outlook on Water Use, Center for Environmental Systems Research, University of Kassel, Final Report, EEA/RNC/03/007, available at: http://scenarios.ewindows.eu.org/reports/fol949029/fol040583/Water_stress_final_report.pdf, 2004.
Gertena, D., Schaphoffa, S., Haberlandtb, U., Luchta, W., and Sitch, S.: Terrestrial vegetation and water balance – hydrological evaluation of a dynamic global vegetation model, J. Hydrol., 286, 249–270, 2004.
Gleeson, T., Wada, Y., Bierkens, M. F. P., and van Beek, L. P. H.: Water balance of global aquifers revealed by groundwater footprint, Nature, 488, 197–200, available at: http://www.nature.com/nature/journal/v488/n7410/abs/nature11295.html#supplementary-information, (last access: November 2012), 2012.
Gleick, P.: Water use, Annu. Rev. Env. Resour., 28, 275–314, doi:10.1146/annurev.energy.28.040202.122849, 2003.
Hanasaki, N., Kanae, S., and Oki, T.: A reservoir operation scheme for global river routing models, J. Hydrol., 327, 22–41, doi:10.1016/j.jhydrol.2005.11.011, 2006.
Hanasaki, N., Kanae, S., Oki, T., Masuda, K., Motoya, K., Shirakawa, N., Shen, Y., and Tanaka, K.: An integrated model for the assessment of global water resources – Part 1: Model description and input meteorological forcing, Hydrol. Earth Syst. Sci., 12, 1007–1025, doi:10.5194/hess-12-1007-2008, 2008.

HESSD
10, 3327–3381, 2013

Hargreaves, G. H. and Allen, R. G.: History and evaluation of Hargreaves evapotranspiration equation, J. Irrig. Drain. E-ASCE, 129, 53–63, 2003.
Hargreaves, G. L., Hargreaves, G. H., and Riley, J. P.: Irrigation water requirements for Senegal River Basin, J. Irrig. Drain. E-ASCE, 111, 265–275, 1985.
Hejazi, M., Edmonds, J., Chaturvedi, V., Davies, E., and Eom, J.: Scenarios of global municipal water use demand projections over the 21st century, Hydrolog. Sci. J., in press, 2013a.
Hejazi, M., Edmonds, J., Clarke, L., Kyle, P., Chaturvedi, V., Davies, E., Wise, M., Patel, P., Eom, J., and Calvin, K.: Long-term global water use projections using six socioeconomic scenarios in an integrated assessment modeling framework, Technol. Forecast. Soc., in review, 2013b.
Hejazi, M. I., Edmonds, J., Clarke, L., Kyle, P., Davies, E., Chaturvedi, V., Wise, M., and Patel, P.: Integrated assessment of global water scarcity over the 21st century – Part 2: Climate change mitigation policies, Hydrol. Earth Syst. Sci. Discuss., 10, 3383–3425, doi:10.5194/hessd-10-3383-2013, 2013c.
Held, I. M. and Soden, B. J.: Robust responses of the hydrological cycle to global warming, J. Climate, 19, 5686–5699, doi:10.1175/jcli3990.1, 2006.
Hoff, H., Falkenmark, M., Gerten, D., Gordon, L., Karlberg, L., and Rockström, J.: Greening the global water system, J. Hydrol., 384, 177–186, doi:10.1016/j.jhydrol.2009.06.026, 2010.
Huntington, T. G.: Evidence for intensification of the global water cycle: review and synthesis, J. Hydrol., 319, 83–95, doi:10.1016/j.jhydrol.2005.07.003, 2006.
Islam, M., Oki, T., Kanae, S., Hanasaki, N., Agata, Y., and Yoshimura, K.: A grid-based assessment of global water scarcity including virtual water trading, Water Resour. Manag., 21, 19–33, doi:10.1007/s11269-006-9038-y, 2007.
Kaczmarek, Z.: Water balance model for climate impact assessment, Acta Geophys. Pol., 61, 423–437, 1993.
Kuhl, S. C. and Miller, J. R.: Seasonal River Runoff Calculated from a Global Atmospheric Model, Water Resour. Res., 28, 2020–2039, 1992.
Liang, X., Lettenmaier, D. P., Wood, E. F., and Burges, S. J.: A simple hydrologically based model of land surface water and energy fluxes for general circulation models, J. Geophys. Res., 99, 14415–14428, doi:10.1029/94jd00483, 1994.
Liang, X., Lettenmaier, D. P., and Wood, E. F.: One-dimensional statistical dynamic representation of subgrid spatial variability of precipitation in the two-layer variable infiltration capacity model, J. Geophys. Res., 101, 21403–21422, doi:10.1029/96JD01448, 1996.

HESSD
10, 3327–3381, 2013

Liu, J. and Yang, H.: Spatially explicit assessment of global consumptive water uses in cropland: green and blue water, J. Hydrol., 384, 187–197, 2010.
Liu, J., Williams, J. R., Zehnder, A. J. B., and Yang, H.: GEPIC – modelling wheat yield and crop water productivity with high resolution on a global scale, Agr. Syst., 94, 478–493, 2007.
Liu, J., Zehnder, A. J. B., and Yang, H.: Global consumptive water use for crop production: the importance of green water and virtual water, Water Resour. Res., 45, W05428, doi:10.1029/2007WR006051, 2009.
Manabe, S.: Climate and the circulation. Part I: the atmospheric circulation and the hydrology of the Earth's surface, Mon. Weather Rev., 97, 739–774, 1969.
Miller, J. R. and Russell, G. L.: The impact of global warming on river runoff, J. Geophys. Res., 97, 2757–2764, 1992.
Milly, P., Dunne, K., and Vecchia, A.: Global pattern of trends in streamflow and water availability in a changing climate, Nature, 438, 347–350, 2005.
Mitchell, T. D. and Jones, P. D.: An improved method of constructing a database of monthly climate observations and associated high-resolution grids, Int. J. Climatol., 25, 693–712, doi:10.1002/joc.1181, 2005.
Mitchell, T. D., Carter, T. R., Jones, P. D., Hulme, M., and New, M.: A Comprehensive Set of High-Resolution Grids of Monthly Climate for Europe and the Globe: the Observed Record (1901–2000) and 16 Scenarios (2001–2100), Tyndall Centre for Climate Change Research, University of East Anglia, Norwich, UK, 30 pp., 2004.
Monfreda, C., Ramankutty, N., and Foley, J. A.: Farming the planet: 2. Geographic distribution of crop areas, yields, physiological types, and net primary production in the year 2000, Global Biogeochem. Cy., 22, GB1022, doi:10.1029/2007gb002947, 2008.
Niu, G.-Y., Yang, Z.-L., Dickinson, R. E., and Gulden, L. E.: A simple TOPMODEL-based runoff parameterization (SIMTOP) for use in global climate models, J. Geophys. Res., 110, D21106, doi:10.1029/2005JD006111, 2005.
Oki, T. and Kanae, S.: Global hydrological cycles and world water resources, Science, 313, 1068–1072, doi:10.1126/science.1128845, 2006.
Oki, T., Nishimura, T., and Dirmeyer, P.: Assessment of land surface models by runoff in major river basins of the globe using Total Runoff Integrating Pathways (TRIP), J. Meteorol. Soc. Jpn., 77, 235–255, 1999.
Oki, T., Agata, Y., Kanae, S., Saruhashi, T., Yang, D., and Musiake, K.: Global assessment of current water resources using total runoff integrating pathways, Hydrolog. Sci. J., Special

HESSD
10, 3327–3381, 2013

issue: Can science and society avert the world water crisis in the 21st century?, 46, 983–995, doi:10.1080/02626660109492890, 2001.
Portmann, F., Siebert, S., Bauer, C., and Döll, P.: Global data set of monthly growing areas of 26 irrigated crops, University of Frankfurt, Germany, 2008.
Ramankutty, N., Evan, A. T., Monfreda, C., and Foley, J. A.: Farming the planet: 1. Geographic distribution of global agricultural lands in the year 2000, Global Biogeochem. Cy., 22, GB1003, doi:10.1029/2007gb002952, 2008.
Raper, S. C. B., Wigley, T. M. L., and Warrick, R. A.: Global sea level rise: past and future, in: Sea-Level Rise and Coastal Subsidence: Causes, Consequences and Strategies, edited by: Milliman, J. D. and Haq, B. U., Kluwer Academic, Dordrecht, 11–46, 1996.
Rost, S., Gerten, D., Bondeau, A., Lucht, W., Rohwer, J., and Schaphoff, S.: Agricultural green and blue water consumption and its influence on the global water system, Water Resour. Res., 44, W09405, doi:10.1029/2007wr006331, 2008.
Rowan, T. S. C., Maier, H. R., Connor, J., and Dandy, G. C.: An integrated dynamic modeling framework for investigating the impact of climate change and variability on irrigated agriculture, Water Resour. Res., 47, W07520, doi:10.1029/2010wr010195, 2011.
Siebert, S., Döll, P., Feick, S., Hoogeveen, J., and Frenken, K.: Global Map of Irrigation Areas version 4.0.1, Johann Wolfgang Goethe University, Frankfurt am Main, Germany/Food and Agriculture Organization of the United Nations, Rome, Italy, 2007.
Sperna Weiland, F. C., van Beek, L. P. H., Kwadijk, J. C. J., and Bierkens, M. F. P.: The ability of a GCM-forced hydrological model to reproduce global discharge variability, Hydrol. Earth Syst. Sci., 14, 1595–1621, doi:10.5194/hess-14-1595-2010, 2010.
SRES: Special Report on Emissions Scenarios: a Special Report of Working Group III of the Intergovernmental Panel on Climate Change, edited by: Nakićenović, N. and Swart, R., Cambridge University Press, Cambridge, England, UK, 2000.
Tobler, W., Deichmann, U., Gottsegen, J., and Maloy, K.: The Global Demography Project, National Center for Geographic Information and Analysis, Santa Barbara CA, 1995.
Viviroli, D., Dürr, H. H., Messerli, B., Meybeck, M., and Weingartner, R.: Mountains of the world, water towers for humanity: typology, mapping, and global significance, Water Resour. Res., 43, W07447, doi:10.1029/2006wr005653, 2007.
Vörösmarty, C., Moore III, B., Grace, A., Gildea, M., Melillo, J., and Peterson, B.: Continental scale models of water balance and fluvial transport: an application of South America, Global Biogeochem. Cy., 3, 241–265, 1989.

HESSD
10, 3327–3381, 2013

Vörösmarty, C., Federer, C., and Schloss, A.: Potential evaporation functions compared on US watersheds: possible implications for global-scale water balance and terrestrial ecosystem modeling, J. Hydrol., 207, 147–169, doi:10.1016/s0022-1694(98)00109-7, 1998.
Vörösmarty, C., Green, P., Salisbury, J., and Lammers, R.: Global water resources: vulnerability from climate change and population growth, Science, 289, 284–288, doi:10.1126/science.289.5477.284, 2000.
Wada, Y., van Beek, L. P. H., van Kempen, C. M., Reckman, J. W. T. M., Vasak, S., and Bierkens, M. F. P.: Global depletion of groundwater resources, Geophys. Res. Lett., 37, L20402, doi:10.1029/2010gl044571, 2010.
Wada, Y., van Beek, L., Viviroli, D., Dürr, H., Weingartner, R., and Bierkens, M.: Global monthly water stress: 2. Water demand and severity of water stress, Water Resour. Res., 47, W07518, doi:10.1029/2010wr009792, 2011.
Wang, D. and Hejazi, M.: Quantifying the relative contribution of the climate and direct human impacts on mean annual streamflow in the contiguous United States, Water Resour. Res., 47, W00J12, doi:10.1029/2010wr010283, 2011.
Wide'n-Nilsson, E., Halldin, S., and Xu, C.-Y.: Global water-balance modelling with WASMOD-M: parameter estimation and regionalisation, J. Hydrol., 340, 105–118, 2007.
Wigley, T. M. L. and Raper, S. C. B.: Implications for climate and sea level of revised IPCC emissions scenarios, Nature, 357, 293–300, 1992.
Wigley, T. M. L. and Raper, S. C. B.: Reasons for larger warming projections in the IPCC third assessment report, J. Climate, 15, 2945–2952, doi:10.1175/1520-0442(2002)015<2945:rflwpi>2.0.co;2, 2002.
Wint, G. and Robinson, T.: Gridded Livestock of the World, Report 131, Food and Agriculture Organization (FAO), Rome, 2007.
WMO: Comprehensive Assessment of the Freshwater Resources of the World, Stockholm Environment Institute, Stockholm, Sweden, 1997.
Yang, D., Kanae, S., Oki, T., and Musiake, K.: Expanding the distributed hydrological modelling to continental scale, IAHS Publ., 270, 125–134, 2001.
Yates, D. N.: WatBal – an Integrated Water Balance Model for Climate Impact Assessment of River Basin Runoff, HIIASA International Institute for Applied Systems Analysis Laxenburg, Austria, 1994.
Yates, D. N.: WatBal: an integrated water balance model for climate impact assessment of river basin runoff, Water Resour. Devel., 12, 121–139, 1996.

HESSD
10, 3327–3381, 2013

Zomer, R. J., Trabucco, A., van Straaten, O., and Bossio, D. A.: Carbon, Land and Water: a Global Analysis of the Hydrologic Dimensions of Climate Change Mitigation through Afforestation/Reforestation, International Water Management Institute, Colombo, Sri Lanka, 44 pp., 2006.

HESSD
10, 3327–3381, 2013

Table 1. Summary of literature estimates of global mean annual runoff using both models and data-based estimates at both the global and continental scales.

Reference	Europe	North America	Africa	South Asia	America	Data/model Oceania	Global	Type
Baumgartner and Reichel (1975)	2564	5840	3409	12 467	11 039	2394	37 713	Data
Korzun et al. (1978)	2970	8180	4600	14 100	12 200	2510	44 560	Data
L'vovich (1979)	3110	5960	4225	13 190	10 380	1965	38 830	Data
WMO (1997)	2900	7890	4050	13 510	12 030	2404	42 784	Data
Shiklomanov (1997)	2900	7770	4040	13 508	12 030	2400	42 648	Data
GRDC (2004)	3083	6294	3690	13 848	11 897	1722	40 533	Data
WRI (2005)	6591	7461			12 380	1693	43 219	Data
FAO (AQUASTAT 2010)	6548	6858	3931	12 413	12 380	892	43 022	Data
Oki et al. (2001)	2191	3824	3616	9385	8789	1680	29 485	LSM-TRIP
Weiland et al. (2010)	2175	4803	5099	10 572	10 678	2371	35 698	GCM ensemble
Alcamo et al. (1997)		4333	4057		10 471		33 973	WaterGAP1
Cogley (1998)							42 353	Data
Fekete et al. (2000)	2822	5396	5567	11 425	11 240	1308	37 758	WBM
Fekete et al. (2002)	2772	5892	4517	13 091	11 715	1320	39 307	WBMc
Doll et al. (2003)	2763	5540	3529	11 234	11 382	2239	36 687	GWHM
Gerten et al. (2004)							40 143	LPJ
Wide'n-Nilsson et al. (2007)	3669	7009	3738	13 611	9448	1129	38 605	WASMOD-M
Doll and Fiedler (2008)	3104	6493	4065	13 168	11 310	1272	39 414	WGHM
Weiland et al. (2010)	2143	5249	5573	11 461	11 186	2633	38 245	PCR-GLOBWB
Hanasaki et al. (2010)							41 820	H08
This study	3194	6108	5217	13 066	9854	1148	38 587	GWAM

HESSD
10, 3327–3381, 2013

Table 2. Comparison of total mean annual runoff in each of the 14 GCAM regions with FAO estimates and two other global hydrologic models (WBM and WGHM).

	GCAM Region Name	Area	FAO estimates	Fekete et al. (2000) (WBM)	Fekete et al. (2000) (WBMc)	Doll and Fiedler (2008) (WGHM)	This study
		1000 ha	$km^3 yr^{-1}$	$km^3 yr^{-1}$	$km^3 yr^{-1}$	$km^3 yr^{-1}$	$km^3 yr^{-1}$
1	USA	964 095	2825	2215	2303	2382	2259
2	Canada	998 491	2850	2067	2494	2702	2751
3	Western Europe	456 723	2071	1564	1567		1591
4	Japan	37 791	430	375	380	367	265
5	Australia and NZ	800 977	819	520	545	1057	1016
6	Former Soviet Union	2 230 727	4731	3286	4043		4920
7	China	1 179 691	3395	2126	2608	2267	2475
8	Middle East	559 724	184	160	167		148
9	Africa	3 031 518	3966	5518	4469		5217
10	Latin America	2 051 763	13 575	12 004	12 459		10 899
11	Southeast Asia	637 481	6798	5552	5698		5206
12	Eastern Europe	116 771	273	302	284		333
13	Korea	9965	65	55	60	51	47
14	India	328 726	1280	1264	1491	1435	1399
	Total	13 404 443	43 262	37 008	38 568	39 414	38 527

HESSD
10, 3327–3381, 2013

Table 3. Estimates of Models' departure (RMSE) from FAO (2010) estimates at the country scale (only countries for which all four models have values are used to estimate the RMSE values) and the GCAM scale.

Deviation from FAO (2010) Estimates	WBM Fekete et al. (2000)	WBMc Fekete et al. (2000)	WGHM* Doll and Fiedler (2008)	This study
Country scale	212	187	118	168
GCAM regional scale	905	572	–	956

HESSD
10, 3327–3381, 2013

Table 4. Global grid-based (basin-based) water scarcity results using the annual WSI.

Period	No stress [WSI < 0.1]	Low stress [0.2 ≤ WSI < 0.4]	Moderate stress [0.2 ≤ WSI < 0.4]	High stress [WSI ≥ 0.4]	Remarks
1995–2000	21–62 %	7–37 %	7–27 %	8–48 %	Range of literature
2005	29.5 % (27.7 %)	14.1 % (21.1 %)	14.5 % (22.4 %)	41.9 % (28.9 %)	This study (BAU)
2050	19.9 % (10.7 %)	11.4 % (17.1 %)	13.6 % (17.4 %)	55.1 % (54.7 %)	
2095	12.7 % (7.4 %)	9.1 % (8.2 %)	12.6 % (20.3 %)	65.6 % (64.2 %)	

HESSD
10, 3327–3381, 2013

Table 5. Nomenclature.

PET_d:	Daily potential evapotranspiration in mm day^{-1}
PET_m:	Monthly potential evapotranspiration in mm month^{-1}
n:	Number of days in each month
Ra:	Extraterrestrial solar radiation mm day
T_a:	Average daily temperature in Celsius
T_r:	Range between maximum and minimum daily temperatures in Celsius
G_{sc}:	Solar constant (= 0.0820 MJ m^{-2} min^{-1})
λ:	Corresponding equivalent evaporation to convert Ra from MJ m^{-2} day^{-1} to mm day^{-1} (= 0.408)
J:	Julian day in the year (1–365)
d_r:	Inverse relative distance Earth–Sun
w_s:	Sunset hour angle (in radians)
φ:	Latitude (in radians)
δ:	Solar declination (in radians)

HESSD
10, 3327–3381, 2013

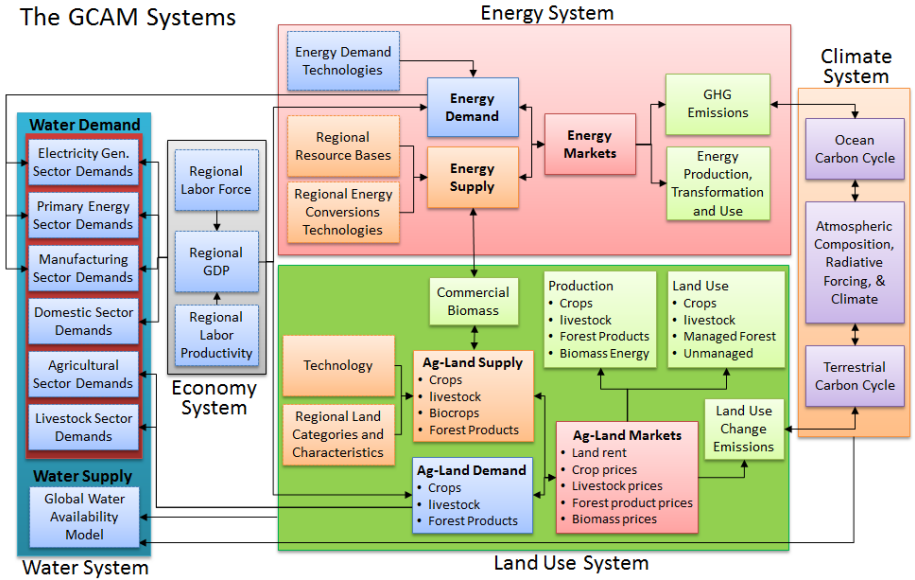

Fig. 1. Schematic of the GCAM systems with links to the water system.

HESSD
10, 3327–3381, 2013

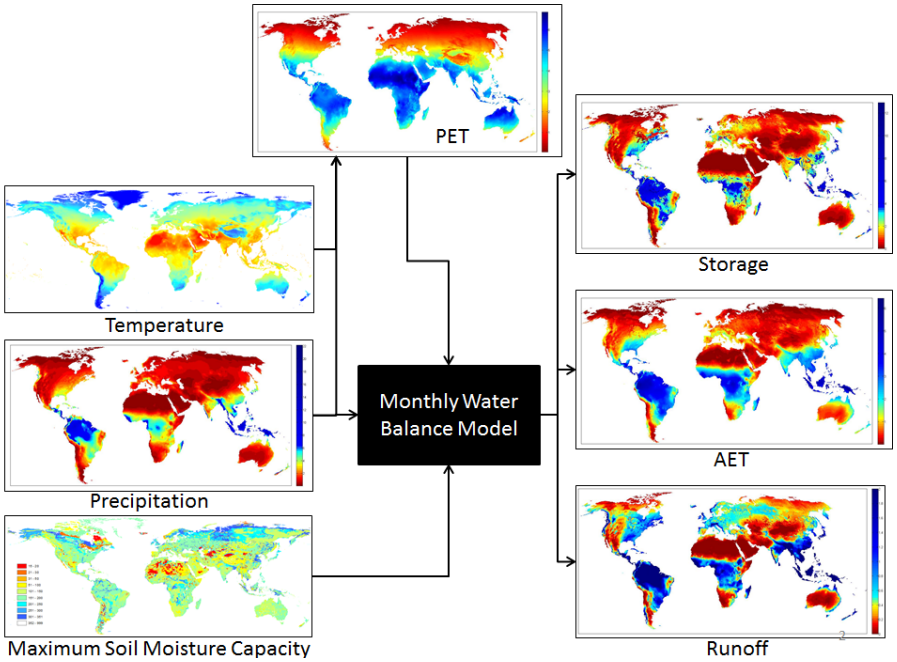

Fig. 2. Schematic of the global water availability model (GWAM) structure.

HESSD
10, 3327–3381, 2013

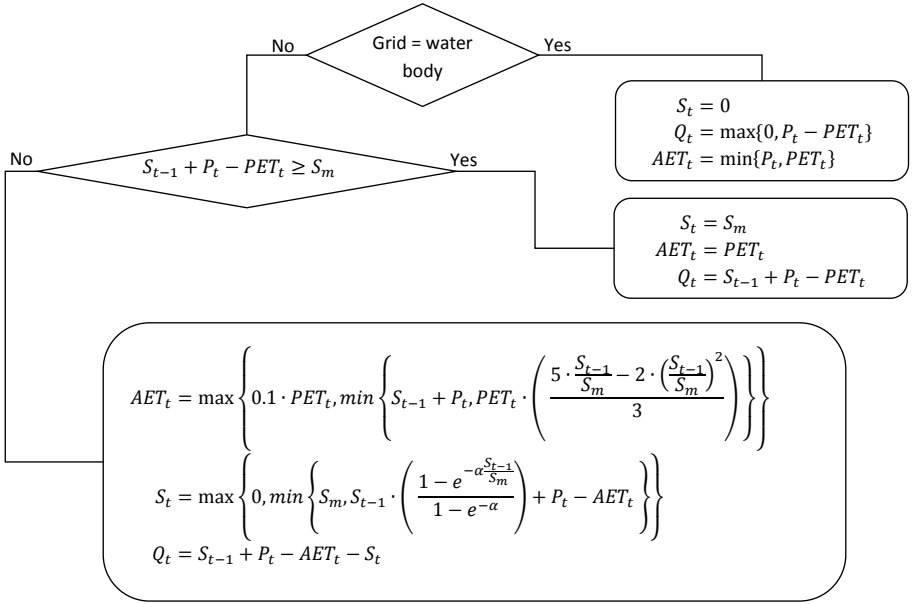

Fig. 3. Flowchart diagram of the monthly water-balance modeling algorithm.

HESSD
10, 3327–3381, 2013

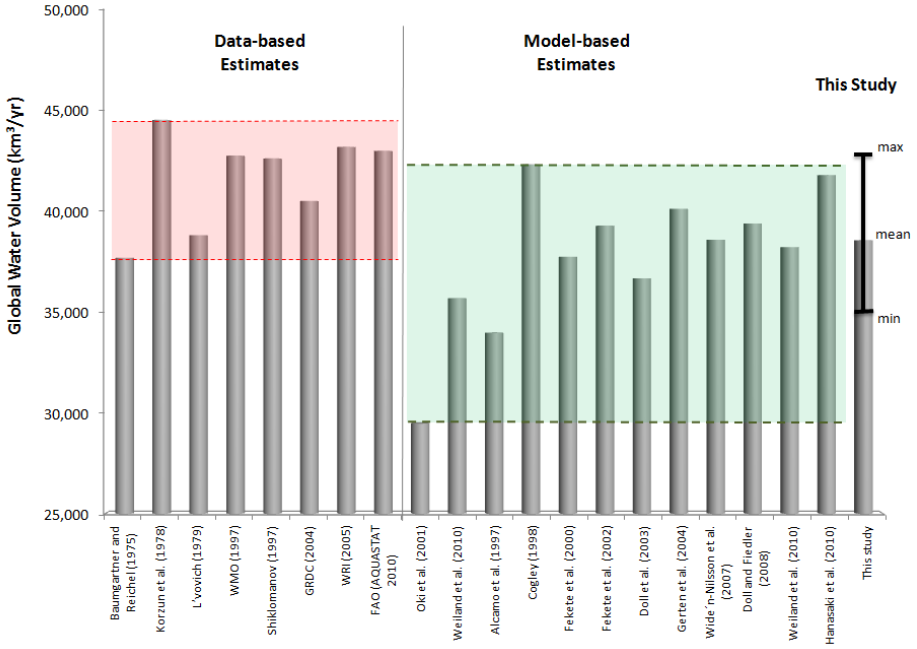

Fig. 4. Comparison of this study's global runoff volume to other data-based and model-based estimates; the bar denotes the highest and lowest simulated runoff.

HESSD
10, 3327–3381, 2013

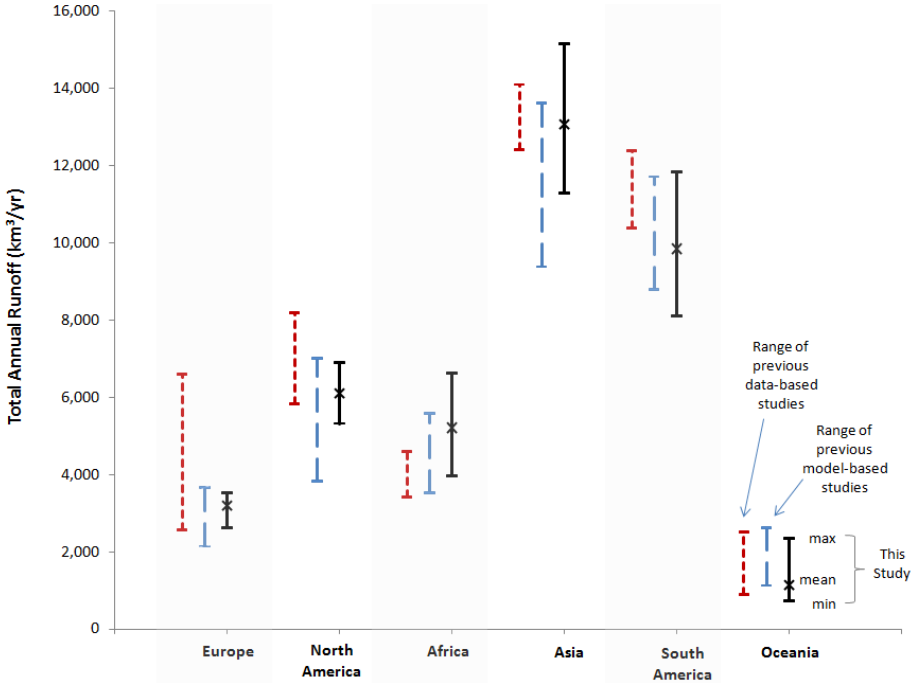

Fig. 5. Comparison of this study's continental runoff volumes to other data-based and model-based estimates; the bar denotes the highest and lowest simulated runoff.

HESSD
10, 3327–3381, 2013

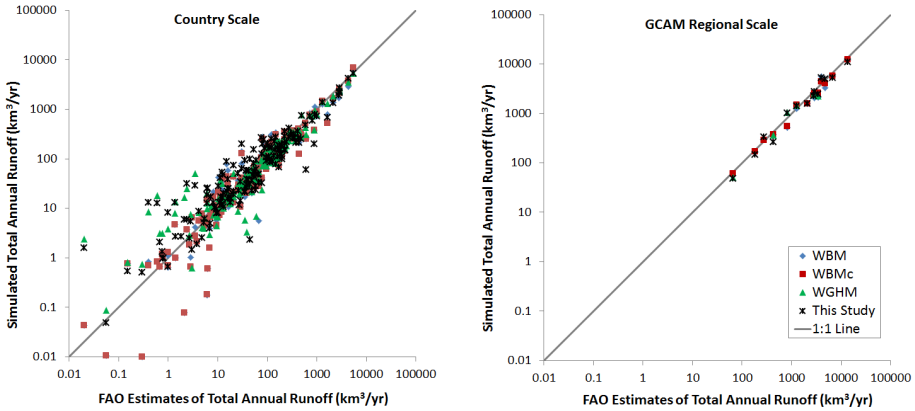

Fig. 6. Comparison of this study's runoff volumes to FAO and other model-based estimates (e.g., WBM, WBMc, and WGHM) at the country and GCAM regional scales.

HESSD
10, 3327–3381, 2013

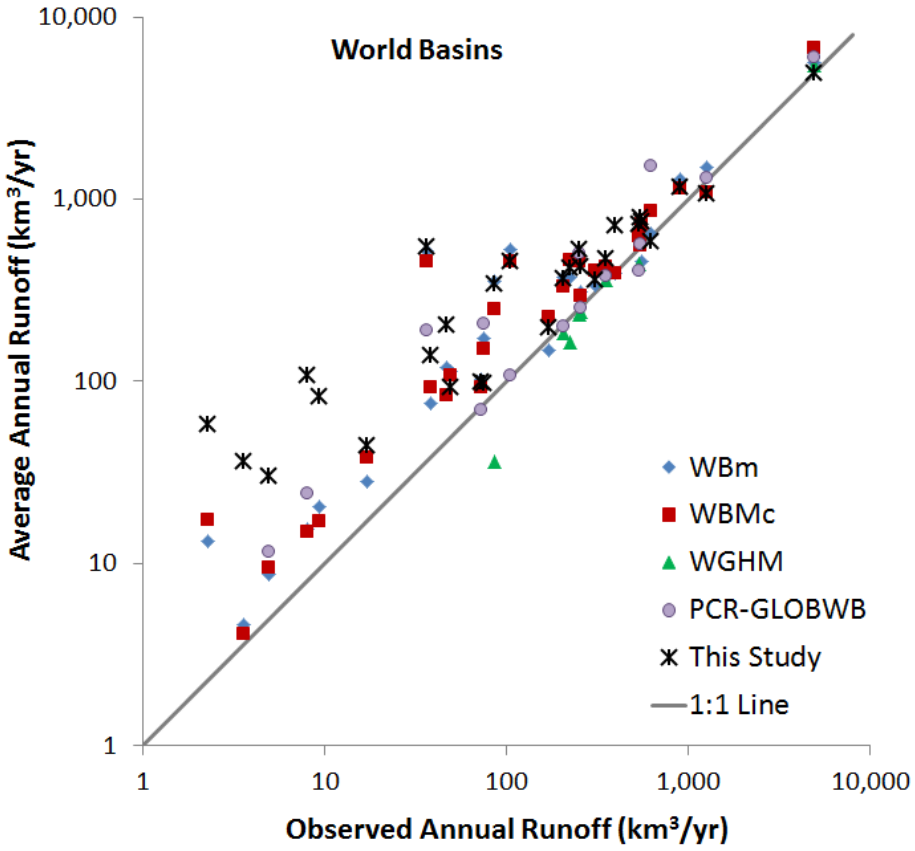

Fig. 7. Comparing simulated runoff for the major basins of the world against observed values (from GRDC).

HESSD
10, 3327–3381, 2013

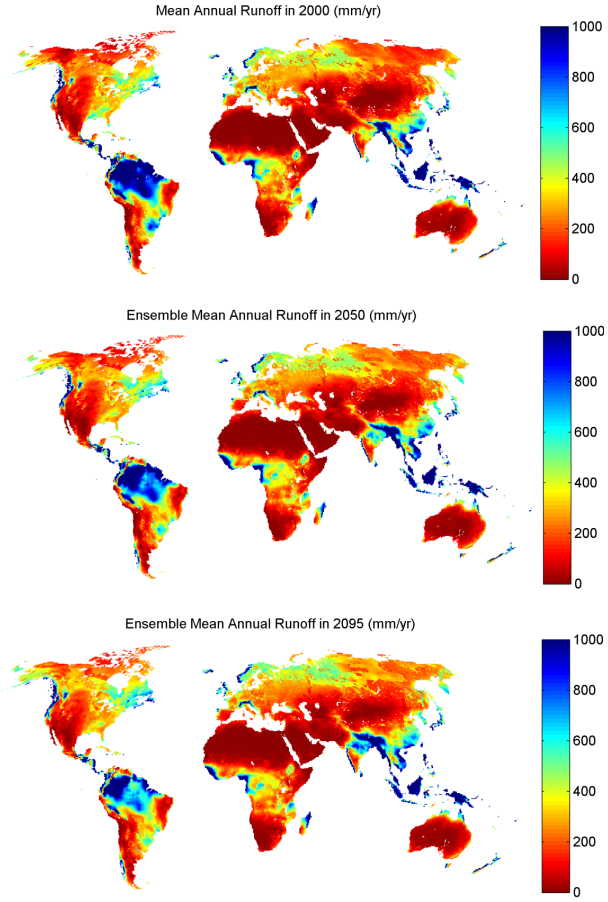

Fig. 8. Ensemble mean annual runoff in year 2005, 2050, and 2095; annual values are averaged over 2001–2010, 2046–2055, and 2091–2100, respectively; ensemble is based on four GCMs and the A1fi emission scenario.

HESSD
10, 3327–3381, 2013

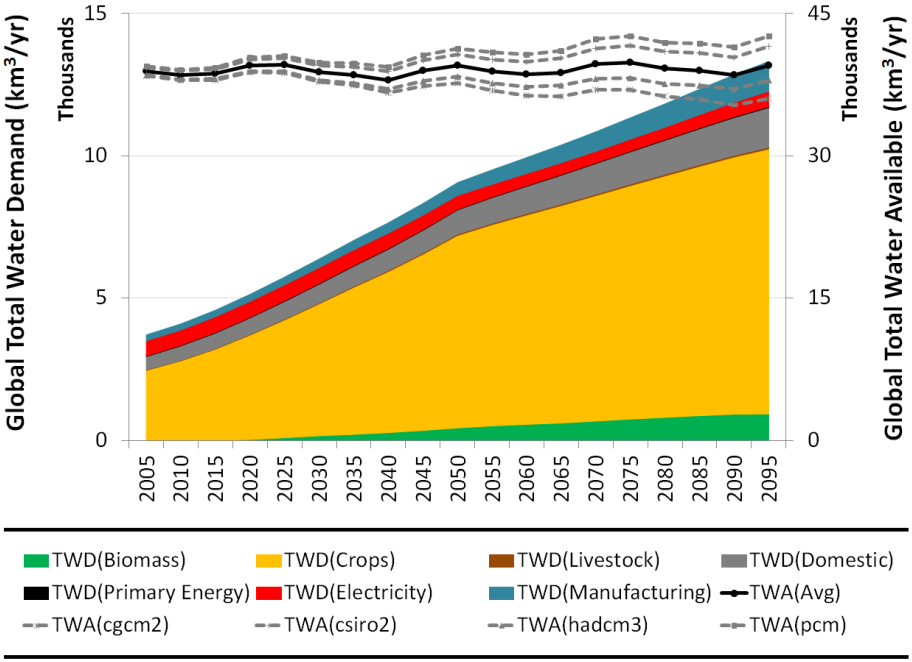

Fig. 9. Global estimates of total water available (TWA) and demand (TWD) over the 21st century; the five lines represent 9-yr moving average of TWA for each of the GCMs (dashed lines) and the mean ensemble (solid line); TWD estimates are broken into their six water demand sectors.

HESSD
10, 3327–3381, 2013

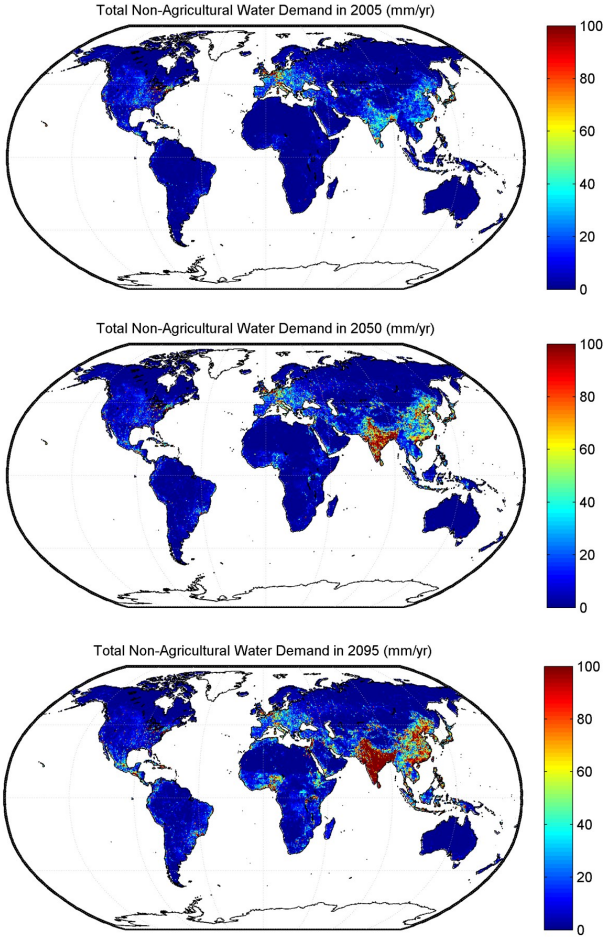

Fig. 10. Total non-agricultural water demand (e.g., municipal, electricity generation, primary energy, manufacturing water demands) in years 2005, 2050, and 2095.

HESSD
10, 3327–3381, 2013

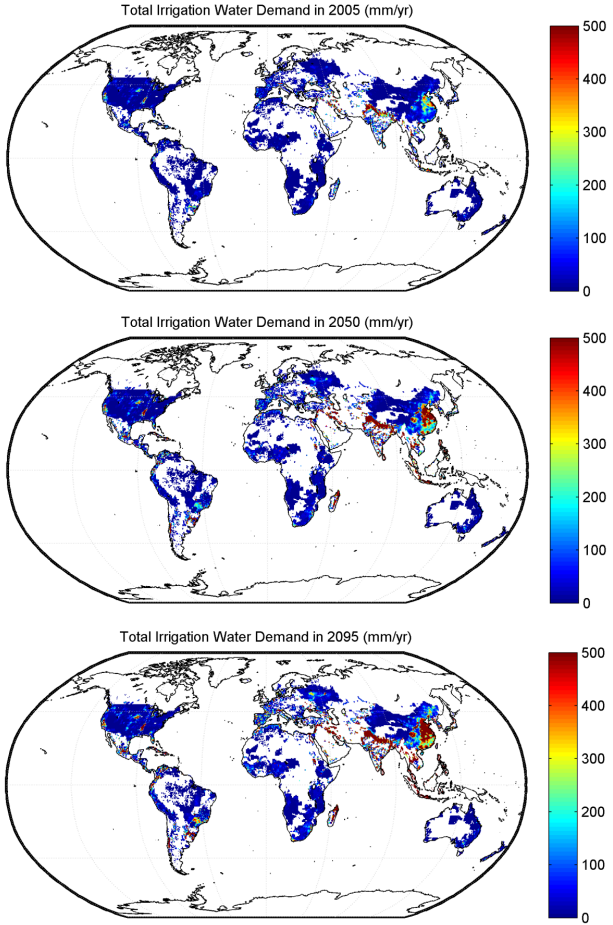

Fig. 11. Total irrigation water demand in years 2005, 2050, and 2095.

HESSD
10, 3327–3381, 2013

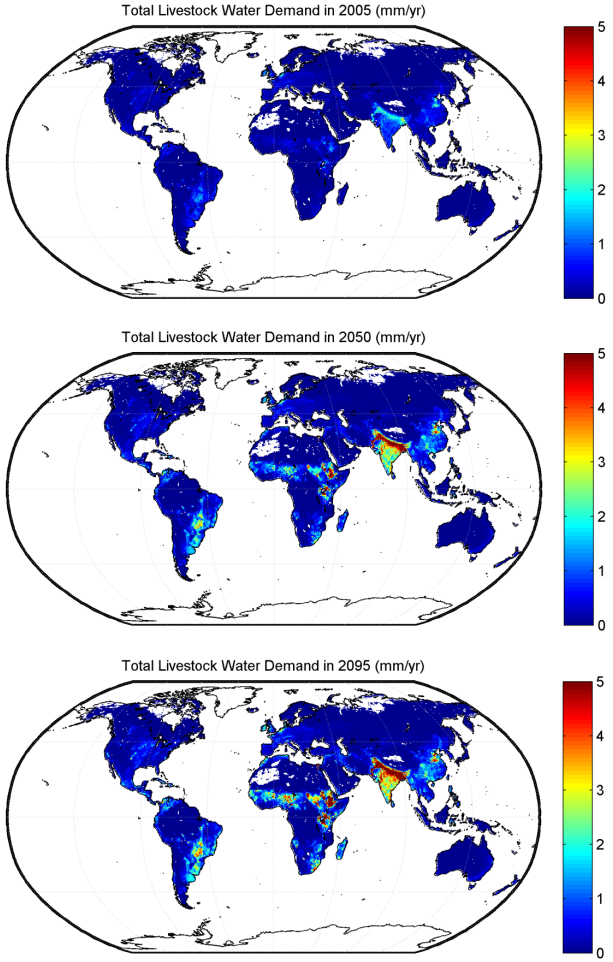

Fig. 12. Total livestock water demand in years 2005, 2050, and 2095.

HESSD
10, 3327–3381, 2013

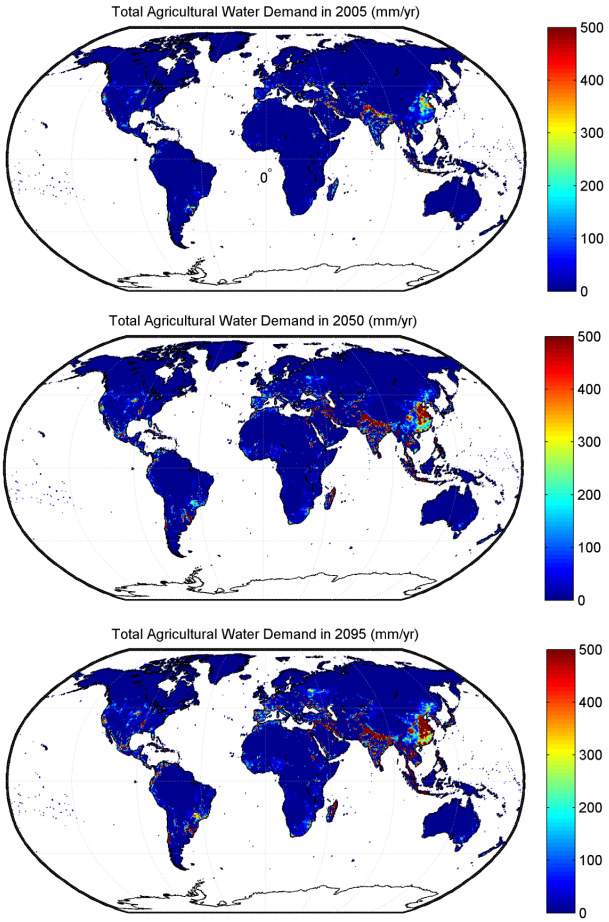

Fig. 13. Total agricultural water demand (e.g., irrigation and livestock) in years 2005, 2050, and 2095.

HESSD
10, 3327–3381, 2013

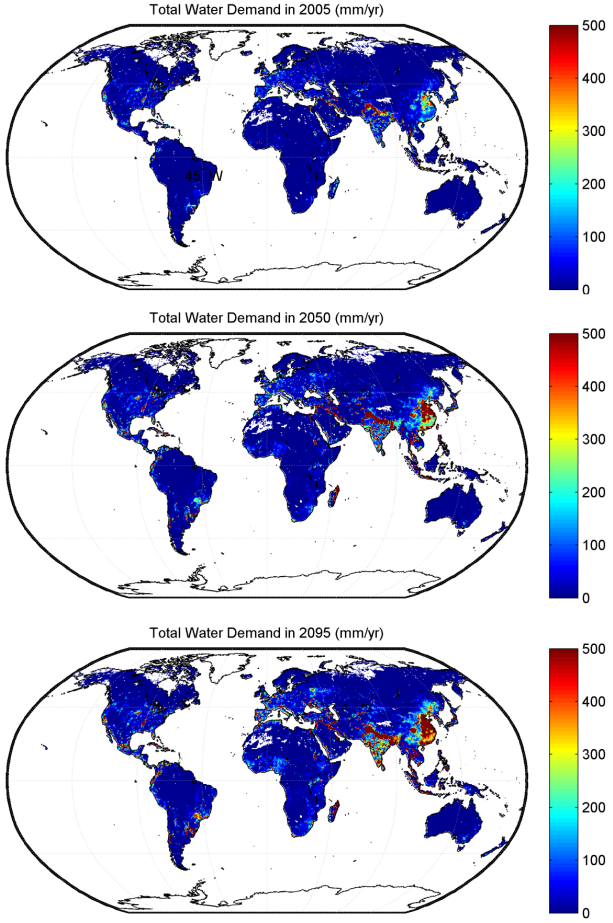

Fig. 14. Total water demand (including both agricultural and non-agricultural sectors) in years 2005, 2050, and 2095.

HESSD
10, 3327–3381, 2013

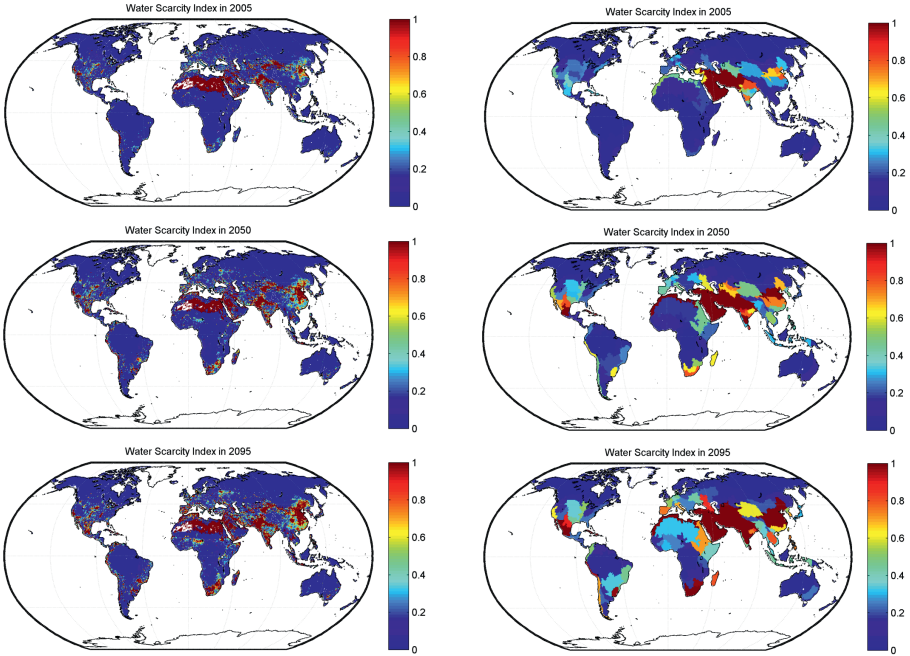

(a) Grid-scale water scarcity

(b) Basin-scale water scarcity

Fig. 15. The water scarcity index (WSI) in years 2005, 2050, and 2095; a value close to one indicates extreme water stress condition while a value close to zero indicates abundant water resources as compared to demands.

HESSD
10, 3327–3381, 2013

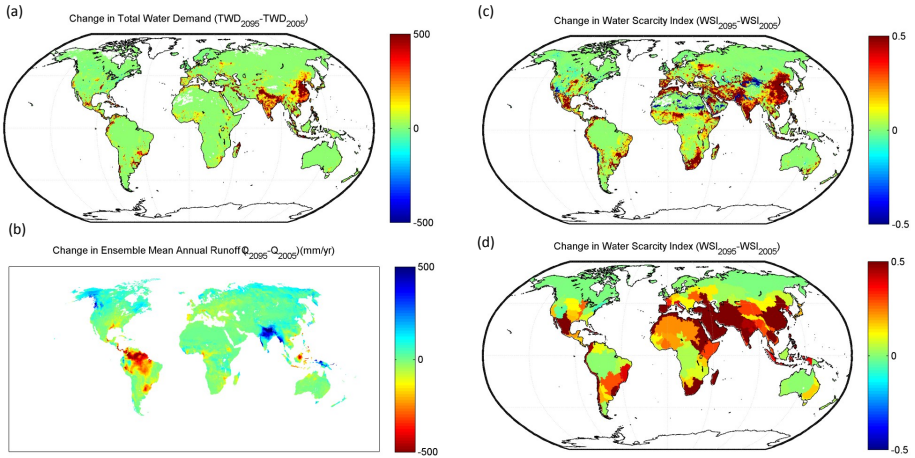

Fig. 16. Change in **(a)** total water demands, **(b)** total water availability, and **(c)** water scarcity index between 2095 and 2005.

HESSD
10, 3327–3381, 2013

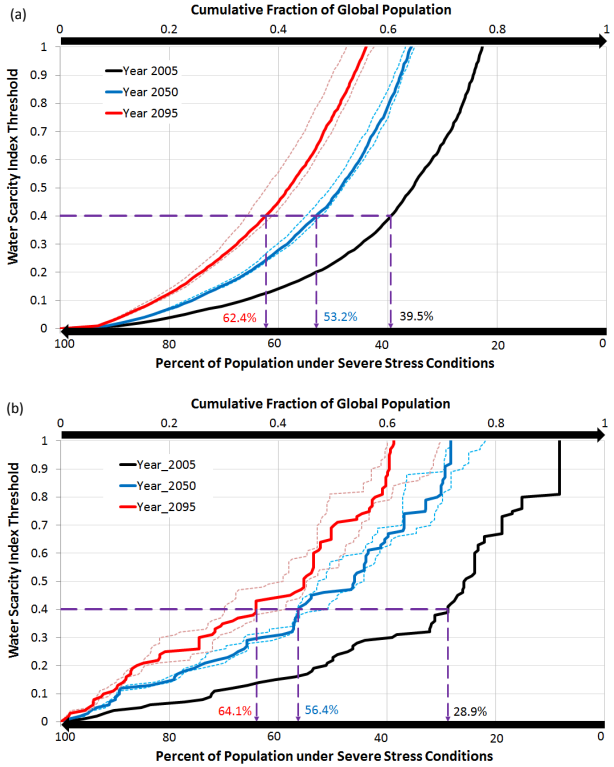

Fig. 17. Shifts to the cumulative probability density function of the fraction of global population living under different levels of scarcity (WSI); water scarcity is estimated at the grid **(a)** and basin **(b)** scales; the thin lines reflect the uncertainty corresponding to the any one of the four GCMs instead of the ensemble mean; global populations living under severe water stress conditions increase from 40 % (29 %) in year 2005 to 53 % (56 %) and 62 % (64 %) in years 2050, and 2095, respectively.

HESSD
10, 3327–3381, 2013

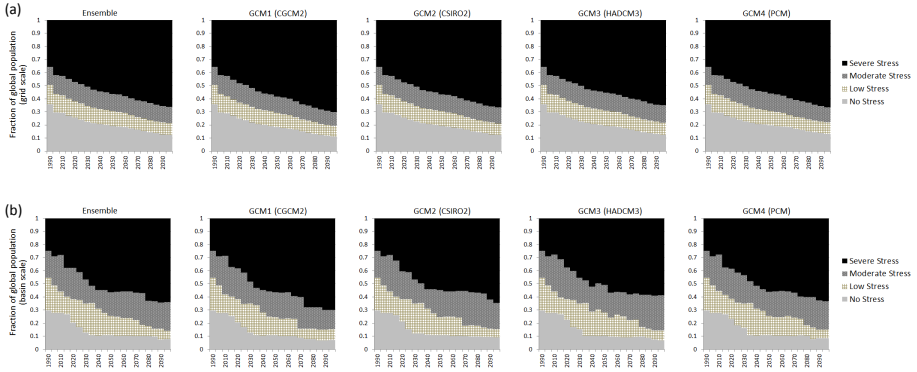

Fig. 18. Distributions of global populations facing each of the four levels of water scarcity conditions: severe stress (WSI ≥ 0.4), moderate stress (0.2 ≤ WSI < 0.4), low stress (0.1 ≤ WSI < 0.2), and no stress (WSI < 0.1); WSI values are computed at the grid **(a)** and basin **(b)** scales and then the shares of populations are aggregated to the global scale.

HESSD
10, 3327–3381, 2013

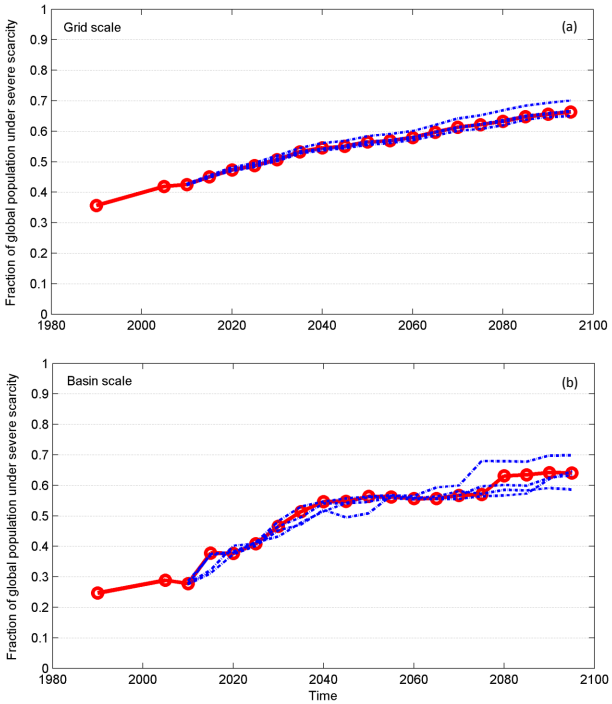

Fig. 19. Estimated percentage of global population living severe water scarcity conditions (WSI ≥ 0.4) at the grid **(a)** and basin **(b)** scales.

HESSD
10, 3327–3381, 2013